pubs.acs.org/Biomac

Article

Characterizing the Molecular Architecture of Hydrogels and Crosslinked Polymer Networks beyond Flory–Rehner—I. Theory

Fernando T. P. Borges, Georgia Papavasiliou, and Fouad Teymour*

Cite This: *Biomacromolecules* 2020, 21, 5104–5118

Read Online

ACCESS | Metrics & More | Article Recommendations

ABSTRACT: In the early 1940s, Paul Flory and John Rehner published a series of papers on the properties of swellable polymeric networks. Originally intended for vulcanized rubber, their development has since been extensively used and extended to much more complex systems, such as hydrogels, and used to estimate the mesh size of such networks. In this article, we take a look at the development of the Flory–Rehner equation and highlight several issues that arise when using such a theory for the described hydrogel networks. We then propose a new approach and equations to accurately calculate the backbone molecular weight in-between crosslinks while explicitly accounting for the molecular mass of the crosslinker and branch segments. The approach also provides more applicable mesh dimensions, for complex networks with macromeric crosslinkers and/or a high degree of branching, as is the case of biocompatible hydrogels. The approach is finally illustrated by a case study comparing the values obtained with our proposed approach to those using the state-of-the-art approach.

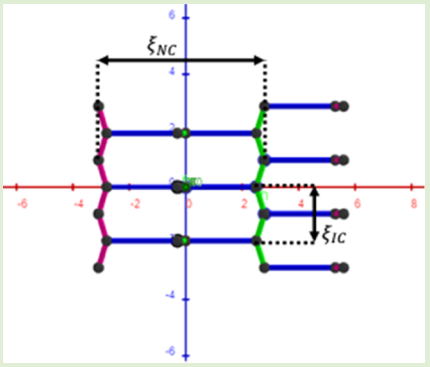

1. INTRODUCTION

Crosslinked polymer networks play an important role as advanced materials across a broad range of industrial applications ranging from tire rubber, to super absorbents, to biomaterials for tissue engineering and drug delivery. Specifically, hydrogels belong to a special class of crosslinked polymers that swell in aqueous media.[1] They are crosslinked networks of hydrophilic polymers that have a large capacity to absorb water and aqueous media and capable of swelling to several times their original volume. Hydrogels used in tissue engineering[2] and controlled drug delivery[3] applications are inherently biocompatible and designed to mimic the properties of human tissue. A recent comprehensive review of biomedical applications of hydrogels, including patent and practice sources, is presented by Calo and Khutoryanskiy.[1]

Since the first synthetic hydrogel made by Wichterle and Lim in 1954,[4] the growth of hydrogel technologies has progressed in a variety of fields,[1] as materials for food additives,[5] pharmaceuticals,[6] and biomaterials, including contact lenses,[7] wound dressings,[8,9] biomedical implants,[10] scaffolds for tissue engineering,[11−16] and controlled drug delivery devices.[17−25] Our research group has focused on the production of poly(ethylene glycol) (PEG)-based hydrogel scaffolds for vascularization of engineered tissues and nanoparticles for sustained release of therapeutic molecules for targeted drug delivery,[21−26] enabled by the use of the bifunctional crosslinking macromer poly(ethylene glycol) diacrylate (PEGDA) within the hydrogel precursor formulation. More specifically, our recent research efforts in drug delivery have focused on the controlled release of biotherapeutics of varying size and conformation that show promise as novel treatments in tissue regeneration, gene delivery, and vaccine development. Examples include peptides,[26,27] polynucleotides, e.g., siRNA,[28] vaccines,[29,30] and possibly plasmids.[31] Encapsulating biomolecules of varying dimensions in hydrogels poses challenges associated with the proper design and size of hydrogel interstitial space. Suitable hydrogel network candidates must not only successfully encapsulate larger biomolecules of interest but also enable their release in a manner consistent with the intended treatment protocol. This is further complicated by the fact that such loosely crosslinked networks, necessary for encapsulation of these biotherapeutics, tend to have compromised mechanical properties.

Therefore, the objectives of this work are to (a) develop a proper methodology for designing hydrogels for encapsulation and release of specific biotherapeutic molecules of varying size, shape, and function, and (b) explore the upper limits of biomolecule size that could be successfully encapsulated and released from hydrogel slabs, microparticles, and nanoparticles.

To achieve these objectives, proper characterization, and understanding, of the properties and molecular architecture of crosslinked polymer networks are crucial. Flory and

Received: August 26, 2020
Revised: November 6, 2020
Published: November 30, 2020

https://dx.doi.org/10.1021/acs.biomac.0c01256
Biomacromolecules 2020, 21, 5104–5118

Rehner[32−34] were first to undertake these tasks in the 1940s. They developed a model that describes the isotropic swelling of crosslinked rubber in the dry state and proposed one of the most commonly known equations in polymer science, the Flory−Rehner (F−R) equation. The Flory−Rehner equation relates the thermodynamic expansion of the network, as expressed by the swelling ratio of the crosslinked polymer, to its characteristic properties and architecture, including the average mass in-between crosslinks, which can easily be translated to the average molecular weight between crosslinks, $\bar{M}_c$. Canal and Peppas[35] utilized the findings of Flory and Rehner and showed that $\bar{M}_c$ can be used to calculate an average distance between crosslinks (in angstroms), referred to as "mesh size". The mesh size has been used as one of the most important properties to characterize a crosslinked polymer network or hydrogel, as it is assumed to correlate to the size of molecules encapsulated for drug delivery.

In spite of being originally developed for characterization of vulcanized rubber,[33] the Flory−Rehner equation has been used extensively to calculate properties of other crosslinked polymer networks, including hydrogels, often without any appreciable change. While this is applicable for the case of hydrogels synthesized from small-molecule monomers like vinyl acetate/alcohol, acrylic acid, hydroxy-ethyl methacrylate (HEMA), vinyl pyrrolidone, acrylamide, lactic acid, silicones, and others much like vulcanized rubber, it might not work as well for cases where high crosslinker ratios are required for encapsulation and release of biotherapeutics of large dimensions and of specific conformations. The usage of macromeric monomers and/or crosslinkers, such as PEGDA, polysaccharides, collagen, chitosan, and hyaluronic acid, and the fairly high crosslinker ratios often used in biomedical applications[17,36−40] make the conformation of these hydrogel networks fairly distinct from that envisioned by Flory and Rehner for vulcanized rubber. In fact, many publications have observed the limitations of applying the Flory−Rehner theory,[41−45] especially when describing networks formed with a macromeric crosslinker and/or in high crosslinker concentrations.[44,45]

Therefore, in this paper, we adopt a different approach to extend the interpretation of results calculated from the Flory−Rehner equation to introduce and calculate new measures of network "mesh" dimensions that are more relevant for hydrogels with macromeric crosslinkers and/or high crosslinker concentrations. These dimensions are of special interest to those applications at the forefront of biomedical and pharmaceutical research that continue to seek the encapsulation and delivery of novel biotherapeutics that involve the use of molecules that are not only significantly larger than current therapeutics but also deviate significantly in their shape and conformation from the traditional assumption of small coiled spheres.

It is important to note that the theoretical developments and equations developed and presented in this paper constitute only a new interpretation of the Flory−Rehner equation and, in no way, question the validity of their approach. After presenting the conceptual development of our approach, we use the kinetic model developed by Lee et al.[38] to simulate a case study of hydrogels with varying formulations to exemplify the extensions that our proposed approach offers beyond the Flory−Rehner methodology and results.

2. METHODOLOGY

2.1. Background. *2.1.1. Flory−Rehner (F−R) Approach.* Flory and Rehner, in their original paper on crosslinked polymer networks,[32] define crosslink points as tetrafunctional centers where the ends of four backbone (BB) segments, termed "chains" in the F−R approach, meet. At the other end of each of the four BB segments, another crosslink is located. Flory−Rehner labels these crosslinks as "nearest neighbors" and indicates that the most probable configuration for these, on average, is at the corners of a regular tetrahedron centered around the aforementioned crosslink. We should note that, in developing the concept of an elementary regular tetrahedral "cell" as a representative unit of the network structure, F−R assumes that "the actual network can be replaced by one in which all of the chains are of the same contour length" and that "the properties of the network can be computed from those of this average cell".[32] This cell is rendered as the regular tetrahedron ABCD centered around point O, in Figure 1a. F−R assumes that the nearest-neighbor crosslinks are fixed at their most probable average positions imposed by the network restraints and residing at the tetrahedral corners, A, B, C, and D. The four chains emanating from these corners meet at the crosslink point P (not shown in the figure), which can occupy a range of positions in the vicinity of O. Only at full extension, i.e., in the fully swollen configuration, would O and P coincide, and then the BB segments (chains) would align with the segments AO, BO, CO, and DO. Thus, at full extension, the angle between any two segments is always going to be equal to the tetrahedral angle of 109.47°. It is also useful, for the purpose of our concept development later in this section, to note that the tetrahedron ABCD can be inscribed in a sphere of radius R (R = AO = BO = CO = DO), equal to the average length of a BB segment.

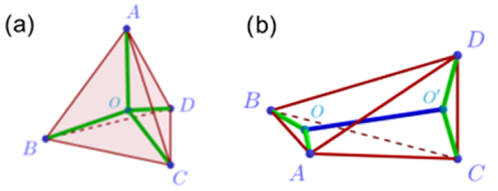

Figure 1. (a) Rendering of the tetrahedron cell described by Flory and Rehner[32] for a crosslinker of negligible size and (b) rendering of the tetrahedron cell for the case where the crosslinker segment is 2.5 times larger in size than the backbone segment.

The Flory−Rehner analysis then utilizes a thermodynamic statistical mechanics approach applied to the tetrahedral representative cell to predict the elastic deformation and swelling behavior of the crosslinked network.[32,33] In doing so, it establishes a relationship between the molecular architecture of the crosslinked network and its macroscopic properties and provides insight into the important factors that govern both. While we refer the reader to the original articles for details on the methodology, we will review and summarize some of its aspects that are necessary for the conceptual development presented here. We will only focus on the process of swelling under the action of solvents and specifically at the limit of equilibrium swelling.

Flory and Rehner postulate that the total change in free energy of the system (ΔG) during the process of swelling under the action of a solvent can be expressed as the sum of

https://dx.doi.org/10.1021/acs.biomac.0c01256
Biomacromolecules 2020, 21, 5104−5118

the change in free energy of mixing (ΔG_{mix}) and the change in elastic free energy (ΔG_{el})

$$\Delta G = \Delta G_{mix} + \Delta G_{el} \tag{1}$$

where ΔG_{mix} for mixing between a polymer and a solvent can be calculated by the Flory–Huggins lattice theory and when no un-crosslinked chains coexist with the network, it is given by eq 2.[46] Note that we are using the equations as presented by Peppas and Barr-Howell[46] for uniformity with our nomenclature and derivation

$$\Delta G_{mix} = kT[n_1 \ln(\phi_1) + \chi_1 n_1 \phi_2] \tag{2}$$

In eq 2, ϕ_1 and ϕ_2 represent the volume fractions of the solvent and polymer, respectively, n_1 denotes the moles of solvent, and χ_1 is the Flory interaction parameter.

Additionally, the change in elastic free energy is associated with the change in the elastic entropy of the system, and when isotropy is assumed, it can be calculated via the statistical theory of rubber elasticity

$$\Delta G_{el} = \frac{\nu_e kT}{2}[3\alpha^2 - 3 - \ln(\alpha^3)] \tag{3}$$

where ν_e is the effective number of chains in the network, and α is the expansion factor for isotropic deformation (note that $\alpha = \phi_2^{-1/3}$). Equations 2 and 3 are then used to express the chemical potential of the solvent, and then after several derivation steps and application of that expression at equilibrium swelling conditions, the well-known Flory–Rehner equation is obtained (eq 4). This could ultimately be used to deduce the crosslinking characteristics of the network from the knowledge of its equilibrium swelling properties

$$\frac{1}{\bar{M}_c} = \frac{2}{\bar{M}_n} - \frac{\left(\frac{\bar{v}}{V_1}\right)[\ln(1-\phi_2) + \phi_2 + \chi_1\phi_2^2]}{\phi_2^{1/3} - \frac{\phi_2}{2}} \tag{4}$$

In eq 4, $\bar{M}_c$ is the average molecular weight between crosslinks, $\bar{M}_n$ is the average molecular weight of the linear polymer before crosslinking (i.e. the primary polymer chains), $\bar{v}$ is the specific volume of the polymer, and V_1 is the molar volume of the swelling solvent.

While the Flory–Rehner equation provides a fairly accurate estimate of the molar mass between crosslinks via a thermodynamic estimation of the number of effective chains per unit mass, it has no direct provision for the calculation of the interstitial mesh dimensions. It is the "distance" between crosslinks, rather than molar mass, that matters most in defining the structure of the network's interstitial space. Drug encapsulation and delivery applications naturally depend on that dimensional distance when exploring the feasibility of a hydrogel for the delivery of a drug molecule of specific size and dimensions.

Peppas and co-workers[35,46−50] propose the use of polymer coil physics to estimate the network's characteristic correlation length (ξ), also referred to as the mesh size, from the F–R calculated molar mass between crosslinks. The mesh size, ξ, is calculated under isotropic equilibrium swelling conditions from the root-mean-square, unperturbed, end-to-end distance of the polymer segment between crosslinks, $\langle \bar{r}_0^2 \rangle^{1/2}$, and the expansion factor, α. The mesh size equation is given as

$$\xi = \alpha \cdot \langle \bar{r}_0^2 \rangle^{1/2} = \phi_2^{-1/3}\left(C_n \eta \frac{\bar{M}_c}{M_r}\right)^{1/2} l \tag{5}$$

where η is the number of bonds per repeat unit, l is the average length of a bond, C_n is the Flory characteristic ratio, which is a measure of the flexibility of the chain, and M_r is the average molecular weight of a repeat unit. C_n is defined as the ratio of the square unperturbed distance, or the Kuhn length, to the square of the random flight end-to-end distance.[50] Note that the calculation of M_r requires knowledge of the polymer composition.

The mesh size (ξ), as illustrated in Figure 1a, represents the length of any of the four segments emanating from the corners to the central crosslink, at full extension under equilibrium swelling.

2.1.2. Limitations of the Flory–Rehner-Based Approach. The Flory–Rehner analysis, and the subsequent mesh size calculation, briefly described above involves two aspects that do not generally hold for the class of hydrogels considered here. First, the approach neglects the size of the crosslinker in its calculations. Specifically, each crosslink is represented by a tetrafunctional connection point in the tetrahedron of Figure 1a. This assumption was reasonable for the case of rubber vulcanization, where each crosslink is virtually a S–S bond but does not hold when crosslinkers of molecular weight as high as $10^{51,52}$–20 kDa[53] are used.

Second, the analysis was limited to the usual case of fairly low concentration of a crosslinker of ~0.1–1 mol %. However, as hydrogels continue to find more and more applications in the biomedical field, biocompatible macromeric crosslinkers become more and more attractive alternative monomers resulting in an increase in the ratio of crosslinker to monomer used in some of these processes. For example, Elbert et al.,[36] Borges et al.,[37] and Lee et al.[38] have successfully formed hydrogel formulations that contained as much as 58 mol % PEGDA, while Watkins et al.,[39] Kalakkunnath et al.,[40] and Mason et al.[1717] used 100 mol % of a macromeric crosslinker. In contrast, the crosslinker amounts used in traditional vinyl–divinyl crosslinking copolymerization are typically limited to less than 10 mol % of the divinyl crosslinker. Specifically, the experiments of Li et al.,[54] later modeled by Kizilel et al.,[55] used less than 2.6 mol % ethylene glycol dimethacrylate (EGDMA) in copolymerization with methyl methacrylate (MMA), while Millar et al.[56] and Sederel et al.[57] both formed styrene–divinylbenzene polymer networks using crosslinker concentrations as low as 7 and 8%, respectively.

It is very important to note that whenever high crosslinker concentrations are used in formulations, many of the crosslinker molecules will be reacted at one end only, resulting in the formation of branches along the primary chain. These branches are characterized by the presence of pendant double bonds (PDB) at their free end. While the F–R approach implicitly accounts for those branches in its thermodynamic analysis, it does not directly address their existence and does not provide a mechanism for their characterization and distinction.

Furthermore, the utility of the characteristic length of the network, or mesh size (ξ), derives from the somewhat regular representative cell and is a direct result of the negligible size of the crosslinker. If we apply the same approach to the case involving macromeric crosslinkers, illustrated in Figure 1b, we will observe that two problems arise: (1) while (ξ) represents

https://dx.doi.org/10.1021/acs.biomac.0c01256
Biomacromolecules 2020, 21, 5104−5118

one of the dimensions of the network, it is no longer fully representative of its now "irregular" structure, and (2) the presence of branches of considerable molar mass emanating from the backbone segments (not shown in the figure) complicates the hitherto "almost linear" equivalence between $\bar{M}_c$ and ξ. To clarify this further, imagine two backbone segments of the same $\bar{M}_c$, where both are made via copolymerization of a small vinyl monomer and a large divinyl crosslinker. Further imagine that the polymerization conditions and the precursor composition lead to significant branching in one, whereas the other remains close to a linear polymer segment. Clearly, the latter will have a much larger number of repeat units and a larger mesh dimension, yet examination of $\bar{M}_c$ alone would not indicate that. Thus, what was an assumed equivalence between the two quantities becomes more difficult to intuit.

To account for the actual significant crosslinker size, and for the presence of a large number of branches along the backbone chains, a new representation of the crosslinked network together with a new set of equations are needed. Those are developed and presented in the subsequent section.

2.2. Conceptual Development. *2.2.1. Chain Segment Types and the Primary Chain.* To illustrate the main molecular architecture features of crosslinked networks that we believe are not explicitly addressed by the F−R approach, we need to introduce clear terminology to help distinguish these features. Four types of chain segments can be classified according to their relative location in the network and whether they are elastically deformable under swelling. Figure 2

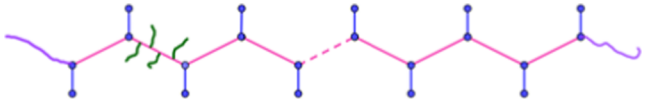

Figure 2. Schematic showing the four different chain segment types, CE (purple), BB (pink), XC (blue), and BR (green), in a polymer network. BR segments are only shown for one BB segment.

considers a single primary chain in the network as a representative example. The primary chain backbone is naturally divided into segments by the crosslinking points; those are termed "chains" in the F−R approach. Of those segments, two are chain ends (CEs) that are constrained only on one side, which could be represented as freely jointed chains. The rest are backbone (BB) segments, which are elastically deformable under shear. The crosslinks (XC) are also polymer chain segments that are elastic under swelling. This is in clear contrast to the classical F−R approach, which considers them as tetrafunctional points. Finally, branched segments (BR) emanate from each backbone segment (including CE) whenever the pendant double bond (PDB) conversion of incorporated crosslinker molecules is not complete. These four types of chain segments are depicted in Figure 2.

2.2.2. Modified Tetrahedral Cell. As illustrated in Figure 1a, central to the Flory−Rehner tetrahedral cell construct is the assumption that the contour length of the crosslink is negligible and can be represented by a point in three-dimensional (3D) space. For the case of a macromeric crosslinker, the length of the crosslinker must be explicitly considered. The crosslink can no longer be confined to a single point O but rather needs to be defined by a segment, O−O′, connecting its reacted double bond ends. Obviously, the crosslink, and its four nearest-neighbor crosslink "ends", cannot be contained in a regular tetrahedron but can now be placed at the vertices of an irregular tetrahedron.

Figure 1b shows an example of this modified tetrahedral cell configuration for an extreme case where the XC segment is 2.5 times larger in size than the BB segment. This extreme case is considered to better illustrate the specific features of this construct. We note that the tetrahedral cell is rendered under conditions of full extension at equilibrium swelling and that it is assumed that the elastic deformation properties of the crosslinker are the same as, or similar to, those of the backbone chains. Deviations from this assumption would necessitate incorporation into the approach and a new derivation for that special case.

As seen in Figure 1b, the angle between any two BB segments (for example, the angle AOB) is altered as compared to the case of the regular tetrahedral cell, where all angles share the value of 109.47°, commonly known as the tetrahedral angle. Furthermore, the change in the value of that angle is a direct result of the introduction of a finite length to the XC segment and consequently depends on the relative contour lengths of BB and XC segments.

A reorientation of the fully swollen tetrahedron cell rendering in three-dimensional space can help simplify the computation of that angle. Without the loss of generality, we will align the XC segment along the x-axis, with one end at the origin, and then place two BB segments in the $x-y$ plane and the other two in the $x-z$ plane. Figure 3a illustrates this

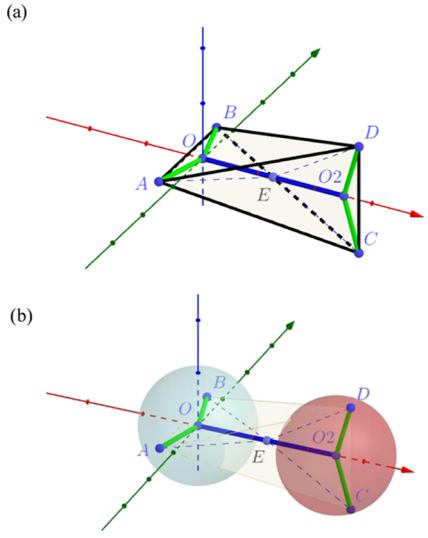

Figure 3. (a) Tetrahedral cell of Figure 1b rotated so that the XC segment is along the x-axis, two BB segments in the $x-y$ plane, and the other two BB segments in the $x-z$ plane; (b) schematic showing the same tetrahedral cell where each pair of BB segments, on both ends of a single XC segment, is inscribed in a sphere of radius equal to the length of a BB segment (x, y, and z axes are depicted in red, green, and blue, respectively).

configuration after reorientation and rotation. It can be easily shown that the orthogonality of the pairs of BB chain segments leads to maximum tetrahedral volume. If either pair is allowed to rotate around the x-axis, the volume will decrease, and thus, this orientation will be preserved throughout the treatment aimed at calculating the value of the angle that maximizes the tetrahedral volume for any given combination of BB and XC lengths.

https://dx.doi.org/10.1021/acs.biomac.0c01256
Biomacromolecules 2020, 21, 5104−5118

As mentioned previously, the original F−R tetrahedral cell (Figure 1a) could be inscribed inside a sphere of radius equal to the BB segment length and centered at O. Inscribing the irregular tetrahedron of Figure 3 in a sphere is equally tractable but does not offer any useful insight. Instead, we elect to inscribe each pair of BB segments in a sphere of radius equal to their fully extended contour length. The resulting arrangement consists of two identical spheres whose centers are separated by a distance equal to the fully extended length of the crosslink XC segment. This arrangement is illustrated in Figure 3b and is essential for the derivation of tetrahedral maximum volume and the expression for the angle that yields it.

We define ξ_{XC} and ξ_{BB} to be the average fully extended length, under equilibrium swelling conditions, of XC and BB segments, respectively, and define x_r to be the ratio between them $x_r = \xi_{XC}/\xi_{BB}$. We also define a as half the angle between two BB segments of the same primary chain (for the case of a regular tetrahedron, $a = 109.47°/2$). The coordinates for the vertices of the tetrahedral cell can be expressed as $A \equiv (-\xi_{BB}\cos(a), -\xi_{BB}\sin(a), 0)$, $B \equiv (-\xi_{BB}\cos(a), \xi_{BB}\sin(a), 0)$, $C \equiv (\xi_{XC} + \xi_{BB}\cos(a), 0, -\xi_{BB}\sin(a))$, and $D \equiv (\xi_{XC} + \xi_{BB}\cos(a), 0, -\xi_{BB}\sin(a))$, and the volume can be calculated as

$$V = \frac{2}{3}\xi_{BB}^{3}\sin^{2}(a)[2\cos(a) + x_r] \tag{6}$$

Under swelling equilibrium conditions, the network will rearrange itself to accommodate as many solvent molecules as it possibly can while simultaneously minimizing its total free energy. In geometric terms, this is equivalent to the maximization of the individual cell volumes. Theoretically, this could be achieved in one of two different ways: (1) the two pairs of BB segments could rotate around the x-axis, but we have already established that volume is maximized when they are confined to orthogonal planes, or (2) the angle between BB segments of the same primary chain ($2a$) changes.

Thus, we can calculate the value of the angle a that maximizes the volume of the tetrahedron by taking the derivative of eq 6 with respect to a and equating it to zero, which, after keeping the root that maximizes volume, leads to this expression for a

$$a = \cos^{-1}\left(\frac{-x_r + \sqrt{x_r^{2} + 12}}{6}\right) \tag{7}$$

Equation 7 shows that, depending on the ratio of the size of the crosslinker to BB segments, the angle between BB segments of the same primary chain will open up further when fully swollen to achieve maximum volume. The value of a ranges from ~54.74 ($2a = 109.47°$) at $x_r = 0$, to 90° ($2a = 180°$) when $x_r \to \infty$ reflecting this observation.

2.2.3. Updating the F−R Thermodynamic Analysis. Turning our attention to the thermodynamic derivation used in the F−R approach,[33,46] we note the use of two volume fractions: ϕ_1, for the solvent, and ϕ_2, for the polymer. To be able to expand their theory to a polymer network composed of both elastically deformable segments (BB and XC) and nonelastically deformable segments (BR and CE), a new accounting of polymer volume fractions is needed. In our approach, we will continue to use ϕ_2 to represent the volume fraction associated with elastically deformable polymer segments but introduce the volume fraction ϕ_3 to represent the nonelastically deformable polymer segments. The definition of ϕ_1 will remain unchanged. We also introduce ϕ_p, the volume fraction of the full polymer network, which is defined as the sum of elastically deformable and nondeformable polymer volume fractions (note that ϕ_p is equivalent to the Flory−Rehner ϕ_2)

$$\phi_p = \phi_2 + \phi_3 \tag{8}$$

It follows that the solvent volume fraction is

$$\phi_1 = 1 - \phi_2 - \phi_3 = 1 - \phi_p \tag{9}$$

In this scheme, the change in free energy of mixing (eq 2) could be updated by accounting for the contribution of both the mixing of the backbone and of the branches with the solvent. Assuming that the Flory−Huggins polymer−solvent interaction parameter is the same for the backbone and for the branches, we write

$$\Delta G_{mix} = kT[n_1\ln(\phi_1) + n_2\ln(\phi_2) + n_3\ln(\phi_3) + \chi_1 n_1\phi_2 + \chi_1 n_1\phi_3] \tag{10}$$

where n_2 is the number of moles of backbone and n_3 is the number of moles of branches. If we then set $n_2 = 0$, as done by Flory and Rehner,[33] and replace $\phi_2 + \phi_3$ by ϕ_p, the equation simplifies to

$$\Delta G_{mix} = kT[n_1\ln(\phi_1) + n_3\ln(\phi_3) + \chi_1 n_1\phi_p] \tag{11}$$

If isotropy is assumed as in the F−R treatment, then the change in elastic free energy continues to be expressed by eq 3. However, care has to be taken to properly update the definition of the expansion factor α and the volume-based swelling coefficient Q_v. Under isotropic expansion, the following relationships hold

$$Q_v = \frac{\text{volume after swelling}}{\text{volume before swelling}} = \frac{\phi_1 + \phi_2 + \phi_3}{\phi_2 + \phi_3} = \frac{1}{\phi_p} = \frac{1}{1 - \phi_1} = \alpha^{3} \tag{12}$$

Therefore, by calculating the change in chemical potential of the solvent and then equating it to zero at equilibrium, as in Peppas and Barr-Howell,[46] a "modified" Flory−Rehner equation is obtained and given by

$$\nu_e = -\frac{[\ln(1 - \phi_p) + \phi_p + \chi_1\phi_p^{2}]}{(V_1/V_o)\left(\phi_p^{1/3} - \frac{\phi_p}{2}\right)} \tag{13}$$

where V_o is the volume of the unswollen (dry) network, V_1 is the molar volume of the solvent, and ν_e is the number of "elastically effective" chains in the network.

Note that the only difference between eq 13 and the F−R equation appears to be a change in notation from ϕ_2 to ϕ_p. However, this difference is not semantic as it accounts for the elastically deformable nature of the crosslink segments XC. Hence, the obtained value of ν_e from eq 13 will, in fact, account for both BB and XC segments, and, therefore, using the Flory−Rehner equation to calculate $\bar{M}_c$, without accounting for XC, would yield overestimated values. Therefore, a new definition for the "elastically effective chain unit" is introduced.

2.2.4. Elastically Effective Chain Unit. Figure 2 clearly shows that every BB segment is accompanied by an XC

https://dx.doi.org/10.1021/acs.biomac.0c01256
Biomacromolecules 2020, 21, 5104−5118

segment. However, since the latter is shared between two primary chains, every BB segment is actually associated with 1/2 of an XC segment. Furthermore, by assuming isotropy in the swelling process and assuming that XC segments have the same expansion factor α as BB segments, then these two segments will maintain a constant size ratio (x_r) and angle between them (the complementary angle of $a/2$) throughout the swelling process, as illustrated in Figure 4.

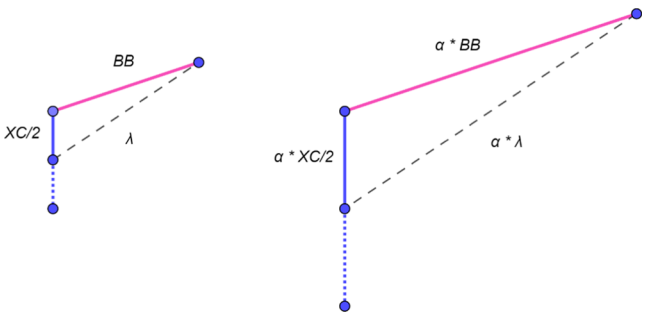

Figure 4. Schematic showing the isotropic swelling of a BB segment and 1/2 of an XC segment, defining the surrogate segment λ.

Thus, a "hypothetical" segment λ, connecting the end of the BB segment to the middle of the XC segment (or the end of the XC/2 segment), can be defined. The segment, λ, geometrically shares the same expansion factor α and is associated with a molecular weight equivalent to the sum of those of the two segments

$$(M_\lambda = M_{tc} + \mathrm{MW}_{XC}/2) \tag{14}$$

where M_{tc} accounts for the total molecular weight between crosslinks, i.e., backbone and branches, and MW_{XC} is the molecular weight of the crosslinking monomer.

In Figure 3, the newly defined segment λ is seen as connecting the middle point of the irregular tetrahedral cell to its vertices, in a similar way that the "chain" segments in the F−R development did for the regular tetrahedral cell. Therefore, λ is actually a surrogate for the new elastically effective chain unit. Thus, ν_e, as calculated in eq 13, is really a measurement of the number of λ segments present in the polymer network. M_λ can be calculated from ν_e, in a way similar to Flory−Rehner's calculation of $\bar{M}_c$.

For a perfect network, it is given by

$$M_\lambda = \frac{V_0}{\nu_e \bar{v}} \tag{15}$$

And for a network where the chain ends are not negligible by

$$M_\lambda = \frac{V_0}{\nu_e \bar{v}}\left(1 - \frac{2M_\lambda}{M_n}\right) \tag{16}$$

Note that, whenever the crosslinker molecular weight is negligible compared to the total molecular weight between crosslinks, M_λ approaches M_{tc} and eqs 13−16 reduce to the Flory−Rehner equations. Otherwise, the knowledge of MW_{XC}, available if the crosslinker is known, allows the calculation of M_{tc} from M_λ. M_{tc} is thus a corrected form of the $\bar{M}_c$ obtained from F−R after accounting for the crosslinker molecular weight; both are inversely proportional to the degree of crosslinking.

2.2.5. Distinguishing Backbone Segments and Branches. While M_{tc} gives a more accurate estimation of the molecular weight in-between crosslinks, to extend the set of equations proposed by Peppas and co-workers[35,46−50] to these networks, we must develop a methodology to differentiate between BB and BR segments. This will allow us not only to calculate the modified mesh dimensions but also to obtain a better understanding of the molecular architecture of those networks.

Recall that BB segments are constrained between two crosslinks and are thus elastically deformable under swelling, while BR segments are restricted on one end, but otherwise free to move inside the aqueous medium of the interstitial space as permitted by the bounds imposed upon them. The number of BR segments per BB obviously depends on the composition of the primary polymer chain or more specifically on the mole fraction of the crosslinker in the polymer, F_x. In fact, calculating the number of branches in between crosslinks, n_{BR}, is the same as calculating the number of crosslinker monomer units in-between crosslinks, n_x, since each of these are crosslinker units that reacted at only one end and thus have an unreacted pendant double bond. Hence, both can be expressed in terms of, n_c, the number of repeat units per BB segment

$$n_{BR} = n_x = F_x n_c = F_x \frac{M_{tc}}{M_r} \tag{17}$$

F_x could be obtained through an additional experimental measurement, a model prediction, or an estimation based on other available information. Various methods are discussed by Borges.[58]

For the sake of subsequent calculation, we will theoretically "sever" the BR branches from the main BB segment. The molecular weight of a branch segment, MW_{BR}, is considered equal to the molecular weight of the crosslinker excluding the end group incorporated into the backbone. For the case of the PEGDA crosslinker, this would be the acrylate group. Thus, the M_{tc} value can be separated into M_{BB}, the molecular weight of the backbone, and M_{BR}, the molecular weight of all branches emanating from that BB segment

$$M_{tc} = M_{BB} + M_{BR} = M_{BB} + n_{BR}\mathrm{MW}_{BR} \tag{18}$$

Note that M_{BB} is the molecular weight of a "linear" elastically deformable backbone segment that shares the same backbone composition and sequence as the original branched total segment between two crosslink points. In our approach, we use M_{BB} to calculate the dimensional distance between crosslinks at equilibrium swelling conditions. We assume that the elastic behavior of this segment is representative of the branched segment it replaces and that we can use its properties to calculate an approximation of its extension length. While this assumption could be valid/acceptable for a range of polymers and branching structures, especially because the backbone is pinned at two ends and the branch is free to move in the solvent, we also recognize that the branches could have an effect on the stiffness, or flexibility, of the backbone. For example, polymers in homologous groups that only differ by the chemical nature of a side group are known to have different values of the Flory characteristic ratio C_n.[59] Thus, whenever the validity of the assumption is suspected, care should be taken to use a value for C_n that is properly suited for the specific polymer.

https://dx.doi.org/10.1021/acs.biomac.0c01256
Biomacromolecules 2020, 21, 5104−5118

Following the same approach of Peppas et al.,[47−50] we can now calculate ξ_{XC} and ξ_{BB}, the average length of a fully swollen crosslinker and backbone segment, respectively

$$\xi_{BB} = Q_v^{1/3} l_{BB} \left(C_{n_{BB}} \eta_{BB} \frac{M_{BB}}{M_{r_{BB}}} \right)^{1/2} \tag{19}$$

and

$$\xi_{XC} = Q_v^{1/3} l_{XC} \left(C_{n_{XC}} \eta_{XC} \frac{MW_{XC}}{M_{r_{XC}}} \right)^{1/2} \tag{20}$$

In the equations above, $M_{r_{BB}}$ is the average molecular weight of the repeat unit in the backbone (excluding branches), and $M_{r_{XC}}$ is the average molecular weight of the repeat unit in the macromeric crosslinker. Note that each segment has its own Flory characteristic ratio ($C_{n_{BB}}$ or $C_{n_{XC}}$), its own average bond length (l_{BB} or l_{XC}), and its own number of links per repeat unit (η_{BB} or η_{XC}). For example, the repeat unit of a PEG-based crosslinker is ethylene oxide (or ethylene glycol) with two C−O bonds and one C−C bond, thus $\eta_{XC} = 3$, and an average bond length should be used. Typically, the BB segment repeat unit is a vinyl monomer with $\eta_{BB} = 2$ and the C−C bond length.

It should be noted that, under certain conditions, the extended segment lengths calculated above might exceed the maximum possible extension for one or both segments. According to polymer physics, the theoretical maximum length a certain polymer chain could reach is the contour length, r_{max}, defined by[60]

$$r_{max} = Nl\cos(\theta/2) \tag{21}$$

Under these conditions, the extended segment lengths need to be corrected. The length of the segment that is fully extended would have to be fixed at the r_{max} value. Naturally, the restriction on expansion of that segment will be countered by excess expansion in the other, such that the resulting overall volume expansion averages out to the value predicted by thermodynamics. A methodology for correcting the expansion of segments under restriction is described by Borges.[58] The corrected segment lengths are labeled ξ_{BB}^{corr} and ξ_{XC}^{corr} in what follows.

Note that, while the restricted expansion phenomenon introduces anisotropy at the molecular level, this effect would not be expressed macroscopically as the orientation of the network segments does not favor any of the spatial dimensions. It averages out in all three dimensions and thus would not be observable at the macroscopic level.

2.2.6. Degree of Crosslinking and Other Properties. The crosslink density, or degree of crosslinking, is another network property of importance. It is generally inversely proportional to the mesh size, or $\bar{M}_c$, or to the newly defined M_λ or M_{tc}. Traditional ways of defining the degree of crosslinking vary as some researchers report a crosslink density expressed as crosslinks per unit volume, or per unit mass, while others use molar fractions. For example, Peppas and Barr-Howell[46] use the first definition and simply calculate it as the polymer density divided by $\bar{M}_c$. While this is of practical use when working with hydrogels in the laboratory, it is of lesser utility when analyzing networks using mathematical models based on polymer reaction engineering principles. Mathematical models, especially those tracking several moments of the molecular weight distribution, conveniently calculate the "fraction of monomers in crosslinks" on the primary chain. Therefore, we will define the gel degree of crosslinking, X_n, as simply the fraction of crosslinks in the primary chain.

To relate this value to quantities generated by this approach, consider a primary chain consisting of m backbone segments. This primary chain would naturally have $m + 1$ crosslinks. Additionally, the primary chain will also have two chain end segments that, for simplicity, we could approximate as one BB segment. The primary chain could thus be represented by $m + 1$ BB segments, each consisting of n_c repeat units, and X_n could be obtained as

$$X_n = \frac{\text{number of crosslinks}}{\text{number of repeat units}} = \frac{m+1}{(m+1)n_c} = \frac{1}{n_c} \tag{22}$$

The approach used in this study also allows for the calculation of additional properties not previously used but of utmost utility for applications involving macromeric crosslinkers. Since we have decomposed the network polymer into BB and BR components, we could start tracking the distribution of volume fraction between them. Swelling experiments yield a knowledge of the polymer volume fraction, ϕ_p. This could be decomposed into ϕ_2 and ϕ_3 using the appropriate molecular weight ratios

$$\phi_2 = \phi_p(M_{BB}/M_{tc}) \tag{23}$$

$$\phi_3 = \phi_p(M_{BR}/M_{tc}) \tag{24}$$

These quantities can be used along with the solvent volume fraction, ϕ_1, to quantify the effect of branches on the reduction of the available interstitial space in the network. This is best discussed through visual exploration of the network.

2.3. Visualization of the Hydrogel Network. Based on the dimensions and properties calculated so far, and with the help of the three-dimensional geometric drawing software GeoGebra, we developed three-dimensional sketches of the polymer network that could provide great insight into its average structure. Figure 5a shows a rendition of a perfect fully swollen network where all of the backbone segment lengths are equal to their average value and the crosslinker length is 2.5 times larger than the backbone segment length. Similarly to Figure 1b this value was selected to magnify the visual effect of the crosslinker size on the network architecture and it is not unreasonable, especially for cases where large amounts of a large crosslinker are used. While we realize that a network with a perfectly repeatable structure is impossible to achieve in reality, this idealized visualization will enable more facile exploration of the characteristic properties of the polymer network. In this regard, the concept is similar to the use of a tetrahedral representative cell by Flory and Rehner.

Figure 5a displays multiple primary chains, some rendered in green and some in pink, depending on their orientation, and XC segments, rendered in blue. The segments are represented by straight lines as the internal details of bond angle configuration along the segments are omitted. Figure 5b shows the projection of the network on the $x-z$ plane. Interestingly, the projection suggests the presence of channel-like hollow structures in the polymer network. These "channels" seen in Figure 5b are a consequence of the assumption of a completely perfect and regular network where every crosslink of a certain primary chain is linked to the same other primary chain. While this is highly unlikely to happen in

https://dx.doi.org/10.1021/acs.biomac.0c01256
Biomacromolecules 2020, 21, 5104−5118

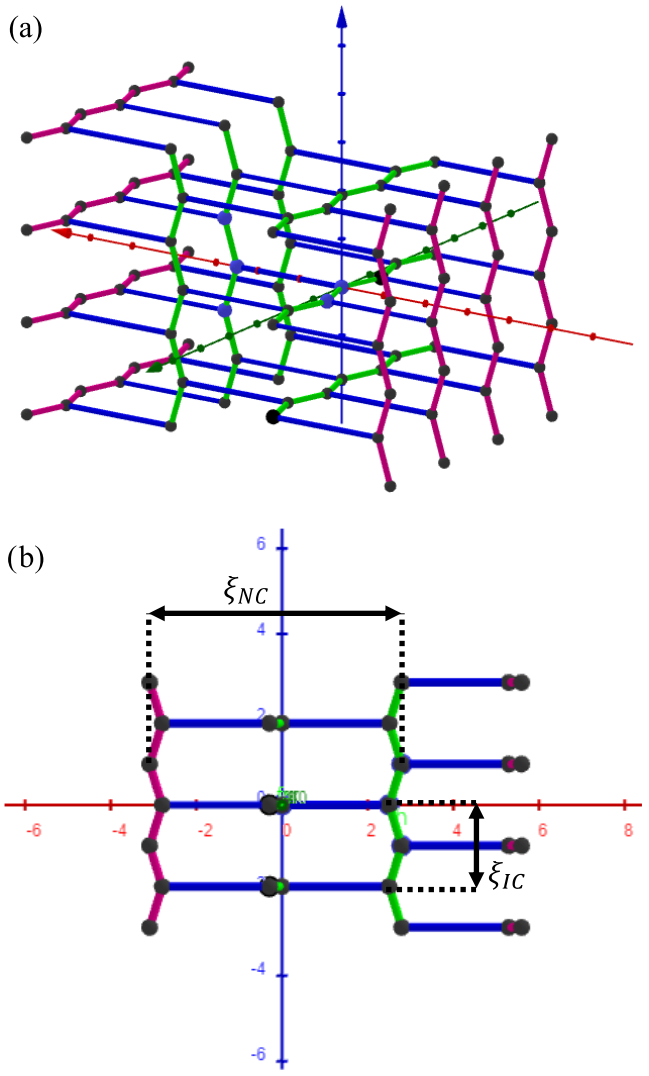

Figure 5. (a) Schematic of the polymer network where the crosslinker segment is 2.5 times larger in size than the backbone segment, and (b) projection on the $x-z$ plane of the polymer network schematic presented in (a) showing the definitions of intrachain mesh distance (ξ_{IC}) and interchain mesh distance (ξ_{NC}).

reality, it actually yields a tighter network, thus providing a conservative estimate of the available space in the network. In imperfect networks, neighboring primary chains will not necessarily only react with each other and, as random crosslinking occurs, the cross-sectional area of these voids is expected to become more complex, and quite larger, than the simple hexagonal polygon shown in Figure 5. This, in turn, allows us to define an upper bound on the size of the molecule to be encapsulated.

In order for a molecule to fit within these network "channels", its dimensions have to be smaller than the dimensions of the cross-sectional area of the "channel", which can be defined by two new dimensional parameters: the intrachain mesh dimension, ξ_{IC}, and the interchain mesh dimension, ξ_{NC}, as marked in Figure 5b. The intrachain mesh dimension, ξ_{IC}, is the average distance between two crosslink points on the same primary chain (therefore, intrachain) that have one crosslink point in between them (or two BB segments). The interchain mesh dimension, ξ_{NC}, is the average distance between two crosslink points on the different primary chains (therefore, interchain) that are in the middle of the two crosslink points that define ξ_{IC} in each primary chain. These dimensions can be calculated by geometric relations

$$\xi_{IC} = 2\xi_{BB} \sin(a) \tag{25}$$

$$\xi_{NC} = 3\xi_{BB} \cos(a) + 2\xi_{XC} \tag{26}$$

Finally, as discussed previously, for the cases where a high crosslinker concentration is used, a high number of branches with unreacted PDBs are present on each BB segment. These would normally take up some of the space available in the "channels", so it is important to quantify this effect. The fraction of the volume taken up by branches, f_{BR}, is defined by

$$f_{BR} = \frac{\phi_3}{\phi_1 + \phi_3} \tag{27}$$

Since branch segments, BR, are constrained on one end only they would be free to move around, and out of the way, to accommodate diffusing molecules. Therefore, we hypothesize that the value of f_{BR} will not restrict the size of the encapsulated molecule. Molecules with dimensions as large as ξ_{IC} by ξ_{NC} should theoretically be able to fit inside the network. However, as the molecule size starts getting closer to the dimensions of ξ_{IC} and ξ_{NC}, diffusion in or out of the network will be more challenging since it needs to be constantly moving BR segments out of its way. This would account for significantly decreased diffusivity. The higher the value of f_{BR}, the larger this hindrance effect on diffusivity is going to be. Future work should focus on experimental and model determination of a correlation between f_{BR} and the diffusivity of various biomolecules in a specific hydrogel network.

A final important point that becomes clear from the visual illustrations in Figure 5, and from the calculated dimensions, is that the size parameter that matters most for the release of a drug molecule from a specific network is not the diameter of the molecule (given by twice its radius of gyration) but rather its projected diameter in the direction of motion. For small spherical, or coiled, molecules, the difference between the two is semantic; however, large biomolecules of interest, including peptides, RNA, and polynucleotides, often have oblong, or elongated, configurations and a nonspherical shape factor. The importance of this observation is that one could hypothesize that fairly large molecules of these types could navigate through relatively narrower "channels" in a hydrogel network as long as their cross section fits within the network void spacing. Their rate of diffusion and advance through these networks would naturally be slow, as they would move in a reptation-like fashion, but they would eventually be released after successfully negotiating all of the obstacles in their paths.

The ideas presented in this paragraph on encapsulation of elongated molecules are currently at the hypothetical stage and will need to be confirmed in properly designed experiments. Success of such experiments would lead to major advancement in biotherapeutic delivery.

3. RESULTS AND DISCUSSION

3.1. Summary of Modified Approach. A step-by-step summary of the application of the new approach is presented in Table 1. Similarly to the state-of-the-art approach, the procedure starts with a measurement of the swelling ratio of the crosslinked polymer and, as previously discussed, an

https://dx.doi.org/10.1021/acs.biomac.0c01256
Biomacromolecules 2020, 21, 5104−5118

Table 1. Summary of Steps and Equations for Proposed Theoretical Approach

#	step	equations
1	measure swelling ratio experimentally and then calculate ϕ_p	$\phi_p = \frac{1}{Q_v}$ $\phi_1 = 1 - \phi_p$
2	use the Flory–Rehner equation to calculate M_λ	$\frac{1}{M_\lambda} = -\frac{(\bar{v}/V_1)[\ln(1-\phi_p) + \phi_p + \chi_1\phi_p^2]}{\phi_p^{1/3} - \phi_p/2}$
3	calculate the total molecular weight in-between crosslinks	$M_{tc} = M_\lambda - MW_{XC}/2$
4	distinguish between branches and backbone segments and calculate M_{BB}	$M_{BB} = M_{tc} - \frac{MW_{BR}F_x M_{tc}}{M_r}$ $M_r = \sum_i F_i MW_i$
5	calculate the average size of a BB and an XC segment at the swelling equilibrium	$\xi_{BB} = \phi_2^{-1/3}\left(C_{n_{BB}}\eta_{BB}\frac{M_{BB}}{M_{r_{BB}}}\right)^{1/2} l_{BB}$ $\xi_{XC} = \phi_2^{-1/3}\left(C_{n_{XC}}\eta_{XC}\frac{MW_{XC}}{M_{r_{XC}}}\right)^{1/2} l_{XC}$
6	compute the angle "a" that maximizes the swollen volume	$x_r = \frac{\xi_{XC}}{\xi_{BB}}$ $a = \cos^{-1}\left(\frac{-x_r + \sqrt{x_r^2 + 12}}{6}\right)$
7	calculate the intrachain and the interchain mesh dimensions	$\xi_{IC} = 2\xi_{BB}\sin(a)$ $\xi_{NC} = 3\xi_{BB}\cos(a) + 2\xi_{xc}$
8	calculate the fraction of the void volume taken up by branches	$f_{BR} = \frac{\phi_3}{\phi_1 + \phi_3}$

estimate of the crosslinker fraction in the polymer, F_x, is also needed. Note that steps 1 and 2 are similar to the application of the traditional Flory–Rehner theory with just a change in notation.

For cases of networks with a macromeric crosslinker used in fairly low amounts (≤1 mol %), it is expected that the effects of branching would be minimal; therefore, $M_{BB} \approx M_{tc}$ and steps 4 and 8 could be omitted. For the cases of networks with small, low-molecular-weight, crosslinkers in large amounts, or of a non-crosslinking macromeric comonomer, the effect of crosslinker size could be neglected but not the effect of branches. In that case, $M_{tc} \approx M_\lambda$, $\xi_{XC} \to 0$, $x_r \to 0$, and $a \to 54.74°$ (regular tetrahedral half-angle) and steps 3 and 6 could be omitted.

Finally, for the case of a network with low-molecular-weight crosslinkers in fairly low amounts, $M_{BB} = M_{tc} = M_\lambda$ and the traditional Flory–Rehner theory applies. Mesh calculations will still differ from Peppas et al.,[35] as the newly defined intrachain and interchain mesh dimensions are calculated. For this case, steps 3, 4, 6, and 8 could be omitted.

3.2. Case Study. Application of the proposed theory, and its special utility for cases of crosslinked networks with significant amounts of macromeric crosslinkers, is illustrated in this section with the help of a case study inspired by our ongoing experimental efforts aimed at validating the methodology. We have conducted a large-scale experimental study using combinations of crosslinker sizes and various precursor composition formulations involving the photoinitiated free-radical copolymerization of ethylene glycol acrylate (EGA) with a PEGDA crosslinker. The study is intended to explore molecular architecture of the hydrogel over a wide range of degree of crosslinking, swellability, backbone branching, and network dimensions. Three variants of PEGDA crosslinker, of molecular weights 575, 2000, and 4600 Da, respectively, were used in various amounts and formulations. A full report on the experimental results is beyond the scope of the present article and will be presented in a companion future publication.

For this case study, we used an approach that generates hydrogel representative "samples" using a mathematical model for the polymerization process to generate realistic $\bar{M}_c$ and F_x values from knowledge of the precursor composition. We then used $\bar{M}_c$ in conjunction with the Flory–Rehner equation (eq 4) to calculate ϕ_p and subsequently combine it with F_x to estimate all network dimensions. This approach has the advantage of connecting the network architecture to the composition of polymer and the selection of crosslinker. A kinetic model, making use of the numerical fractionation technique, which accounts for gelation and accounts for sol and gel properties independently,[61] initially developed by Kizilel et al.[55] and adapted by Lee et al.[38] for photopolymerization, was used. To best represent the polymerization system used in the experimental study, we assumed that the crosslinker and the comonomer were kinetically similar, in spite of the difference in their molecular weights. Thus, the cross-propagation reactivity ratios, r_1 and r_2, for this pair of monomers, were assumed equal to 1. This assumption does not restrict the utilization of our approach in any way as other reactivity ratios could be used whenever available; it does, however, allow us to change the monomer composition, and therefore the properties of the polymer network, without affecting the overall kinetics of the simulation, making it easier to correlate hydrogel properties to precursor composition. Validation of this assumption and all kinetic parameter selections will be presented alongside experimental results in the upcoming publication. The values of the propagation and termination rate constants used in the model were the same for both monomers at 1.84×10^4 and 5.78×10^6 L/(mol·s), respectively. All other parameters, including photoinitiation, were kept at the values reported by Lee et al.[38]

The kinetic model was used to simulate the copolymerization of ethylene glycol acrylate methyl ether (EGA) with PEGDA 575, initiated by the photopolymerization system involving eosin-Y and triethanolamine (TEA) via an argon ion laser (Coherent Innova 70C) producing 78 mW/cm^2 of light at a wavelength of 514 nm. Model results provided the polymer composition, expressed as F_x, and the gel degree of crosslinking, X_n, as defined in eq 22, for varying crosslinker monomer fractions, f_x, ranging from 3 to 93%. Once these two quantities were obtained, the values of n_c and $\bar{M}_c$ were calculated. The values of the expansion factor, α, and of the polymer volume fraction, ϕ_p, were then calculated from $\bar{M}_c$ using eq 4 and assuming water as the solvent (V_1 = 18 mL/mol, χ = 0.426,[62] $\bar{v}$ = 0.89 mL/g[63]). Once the polymer volume fraction, ϕ_p, and therefore Q_v and Q_m, the volume- and mass-based swelling factors, were obtained, the approach summarized in Table 1 was applied to the data and used to calculate the network dimensions. Six formulations were simulated in the kinetic model, and the simulation and F–R results are presented in Table 2, while Tables 3 and 4 summarize the network dimensions, and several other hydrogel properties, calculated using the approach detailed in Table 1, respectively.

https://dx.doi.org/10.1021/acs.biomac.0c01256
Biomacromolecules 2020, 21, 5104–5118

Table 2. Summary of Kinetic Model Simulation Results for Estimation of Swelling Ratios for the Simulated Gels of PEGDA 575

	model calculations			F−R calculations		
f_x	F_x	X_n	$\bar{M}_c$ (g/mol)	Q_m	Q_v	α
0.03	0.05	0.007	24 688.0	15.15	17.97	2.62
0.21	0.30	0.024	11 857.1	10.19	12.41	2.32
0.39	0.51	0.040	9721.0	9.16	11.26	2.24
0.57	0.68	0.053	8897.4	8.74	10.79	2.21
0.75	0.83	0.064	8463.8	8.51	10.54	2.19
0.93	0.96	0.074	8168.4	8.36	10.36	2.18

In the calculations of Tables 3 and 4, the values of $C_{n_{XC}}$ and $C_{n_{BB}}$ were obtained from C_∞ values and varied with the number of links per segment, N,[60] using $C_{\infty_{XC}} = 6.7$[60] and, coincidentally, $C_{\infty_{BB}} = 6.7$.[59] Based on literature recommendations,[60] we assumed $C_n = C_\infty$ for $N > 100$. However, it is important to note that several factors affect the chain flexibility and subsequently the correct values of C_∞ and C_n to be used. Among those, we note that the values reported above are for polymer melts and that C_∞ can change significantly in solution depending on the polymer's affinity to a specific solvent.[59,60] Furthermore, the case study "sample" backbone segments involve copolymers of varying composition, and degree of branching, which necessitates accounting for the effect of composition and side chains on the value of C_∞. The values of η_{XC} and η_{BB} were used as 3 and 2, respectively, while l_{BB} was equal to the length of the C−C bond (l_{BB} = 1.54 Å) and l_{XC} was equal to the average of two C−O bonds (1.42 Å) and one C−C bond (l_{XC} = 1.50 Å). For the calculation of the values of mesh size, ξ, through the F−R/Peppas state-of-the-art approach, l = 1.54 Å and η = 2 were used, while C_n was calculated as before.

Tables 3 and 4 highlight the similarities and differences between the results obtained from the two approaches. In analyzing the similarities, we start by noting that the values of $\bar{M}_c$ and M_{tc} in Table 4 are fairly close. They differ only by a fixed amount equal to one half the molecular weight of the PEGDA 575 crosslinker. While the difference is small for this specific crosslinker, we should duly note that PEGDAs of molecular weight 10−20 kDa are often used in making hydrogels.[51−53] Much more significant differences would be exhibited for those cases. Similarly, we note, in Table 3, that the mesh size, ξ, calculated according to the Peppas et al. approach[35,46−50] is also close in value to the size of the backbone segment, ξ_{BB}, calculated in our approach. Once again, this is not surprising as both approaches attempt to calculate similar distances. Note that their approach requires a value for the average molecular weight of a repeat unit, M_r, which is not readily available for copolymers unless F_x is known as indicated previously.

The similarities stop here as can be seen from the collection of additional metrics calculated by our approach and presented in both tables. Those extend the network analysis beyond the measures characterized traditionally by Flory−Rehner.

In Table 3, we report several network dimensions alongside the size of the backbone segment, ξ_{BB}. These include the size of the extended crosslink segment, ξ_{XC}, the newly proposed interchain and intrachain mesh dimension measures ξ_{IC} and ξ_{NC}, respectively, and the angle between BB segments ($2a$). In contrast, the state-of-the-art approach focuses only on the backbone and completely ignores the size of the crosslinker. Our calculations clearly show that the size of the XC segment is significant compared to that of the BB segment and thus cannot be neglected, even for this case study where a relatively small macromeric crosslinker (MW = 575 g/mol) is used. The ratio of ξ_{XC} to ξ_{BB} varies depending on the degree of crosslinking, increasing as the latter increases, until, at the limit of the tightest crosslinked network in Table 3, ξ_{XC} is actually larger than ξ_{BB}.

The resulting network structure thus deviates significantly from the regular tetrahedral representative cell proposed by Flory−Rehner. This effect is best quantified by the value of the angle $2a$. Recall that the value of this angle for the F−R tetrahedron is 109.47°, and note that all cases in Table 3 exceed this value, starting at 116.1° and increasing to 130° as the degree of crosslinking increases. These results show how the introduction of the nonzero length of the XC segment alters the geometry of the tetrahedral cell and the structure of the polymer network as the backbone segments are forced to open to a wider angle under the influence of the expansion of XC.

The mesh dimension measures ξ_{IC} and ξ_{NC} provide a more accurate representation of the network interstitial space structure than traditional F−R. Notice that the values shown in Table 3 are much larger than the calculated mesh size. Even the intrachain mesh dimension, the smaller of the two in this example, is 70% larger than the mesh size, on average. The interchain dimension, ξ_{NC}, reaches almost twice ξ_{IC} for this case study. For even longer crosslinkers, this ratio will increase drastically, as the interchain dimension is dependent on the size of the crosslinker (cf. eq 26). This is further illustrated, in the following section, through a comparison of cases using different crosslinker molecular weights and is portrayed in Figure 6.

Note that all calculated values of ξ_{XC} in Table 3 are presented in boldface to indicate that they exceed the contour length of XC, thus necessitating a correction for the restricted expansion effect. Furthermore, in the last case, representing the most tightly crosslinked network, the value calculated for BB also exceeds its contour length. The corrected values of the

Table 3. Network Dimensions for the Hydrogel Formulations of Table 2

f_x	ξ (Å)	ξ_{BB} (Å)	ξ_{XC} (Å)	$2a$ (deg)	ξ_{IC} (Å)	ξ_{NC} (Å)	$R_{max_{BB}}$ (Å)	$\xi_{max_{xc}}$ (Å)	ξ_{BB}^{corr} (Å)	ξ_{XC}^{corr} (Å)	$2a$ (deg)	ξ_{IC}^{corr} (Å)	ξ_{NC}^{corr} (Å)
0.03	173.82	172.81	**52.58**	116.1	293.32	379.33	426.72	42.83	175.42	42.83	114.9	295.72	368.84
0.21	78.80	77.87	**46.47**	121.8	136.08	206.57	115.84	42.83	78.77	42.83	120.8	136.99	202.34
0.39	58.68	57.51	**44.99**	125.0	102.05	169.62	69.98	42.83	58.01	42.83	124.3	102.57	166.98
0.57	49.22	48.55	**44.36**	127.2	86.96	153.50	52.53	42.83	48.89	42.83	126.6	87.35	151.59
0.75	43.93	43.19	**44.00**	128.8	77.90	143.98	43.37	42.83	43.35	42.83	128.3	78.04	142.33
0.93	40.64	**39.84**	**43.75**	130.0	72.22	138.02	37.60	42.83	37.59	42.83	130.6	68.29	132.78

https://dx.doi.org/10.1021/acs.biomac.0c01256
Biomacromolecules 2020, 21, 5104−5118

Table 4. Hydrogel Infrastructure Properties for the Hydrogel Formulations of Table 2

f_x	Q_v	$\bar{M}_c$ (g/mol)	M_{tc} (g/mol)	M_{BB} (g/mol)	M_{BR} (g/mol)	$\frac{M_{BR}}{M_{tc}}$	n_c	f_{BR}
0.03	17.97	24 688	24 401	20 514	3887	0.16	161.08	0.01
0.21	12.41	11 857	11 570	4923	6647	0.57	43.73	0.05
0.39	11.26	9721	9434	2655	6779	0.72	26.42	0.07
0.57	10.79	8897	8610	1793	6817	0.79	19.83	0.08
0.75	10.54	8464	8177	1341	6839	0.84	16.37	0.08
0.93	10.36	8168	7881	1059	6822	0.87	14.19	0.09

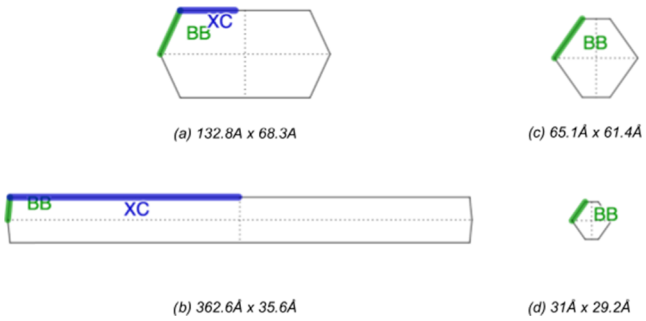

Figure 6. Projection of the internal structure of hydrogel networks on the $x-z$ plane for the two samples of Table 5: panels (a) and (b) are the PEGDA 575 and PEGDA 2000 samples, respectively. Panels (c) and (d) show the equivalent projections when the crosslinker size is neglected. Inter- and intrachain dimensions are noted for each panel. Branches emanating from the BB segments are not shown.

segment lengths and network dimensions that account for the restricted expansion are presented in the final set of columns. Note that, for the first five cases, the error involved in these calculations, with or without the restriction on XC, is minimal. Specifically, the error in the BB segment length is less than 1.5% for all five cases.

Special attention should be given to the last case in Tables 2 and 3, involving a large amount of crosslinker (f_x = 0.93) and exhibiting a relatively high degree of crosslinking. This case presents an extreme scenario in which both BB and XC segments reach their maximum extension at swelling. In handling this extreme case, both ξ_{BB}^{corr} and ξ_{XC}^{corr} must be set to their r_{max} values as the calculation process is sidestepped. This phenomenon seems to indicate that a maximum volumetric swelling ratio exists for any specific hydrogel depending on compositional formulation. Even though this maximum is obtained from polymer physics/geometry, it must be consistent with thermodynamics; thus, extreme extension cases could be used as validation of the approach and parameters used. For example, back-calculation of Q_v yields a value that is ∼14% lower than predicted by applying F−R to the mathematical model results. In comparison, we observed in our experimental study, run in triplicate, the difficulty of reproducible determination of the swelling ratio. The standard deviation of the mass-based swelling ratio, Q_m, in all PEGDA 575 experiments stayed mostly in the range of 5−37%, with an average of ∼13%. Given the maximum extension dimensions for XC and BB, a corrected value of Q_v could be obtained through adjustment of some of the parameters used. We were able to achieve this goal with minimal readjustment of C_n (5.14 instead of 5.84). Experiments based on this phenomenon could be designed for further validation.

Table 4 highlights additional hydrogel network features that provide insight into infrastructure properties extending beyond the mesh and segment dimensions. Of special interest is the fraction M_{BR}/M_{tc} that is seen to increase significantly as the crosslinker content increases, resulting in a larger number of branches emanating from the backbone. As this fraction increases, more of the total mass between crosslinks is located in BR segments than in the backbone. For example, the case of f_x = 0.93 yields a polymer network where 87% of the total molecular weight in-between crosslinks is now in branches, and the backbone molecular weight is ∼1/8 of the $\bar{M}_c$ value predicted by the Flory−Rehner equation. This differentiation allows us to visualize the hydrogel network in a novel way by specifying the concept of a network "skeleton", defined as the elastically deformable backbone segments. The network skeleton is the portion of the polymer that extends under swelling and governs the process of expansion. In the case cited here, it makes up only 13% of the total polymer in this hydrogel example. In traditional F−R analysis of hydrogels, the network "skeleton" comprises all of the polymer in the hydrogel (excluding chain ends). This difference might seem semantic, in light of the fact that both lead to similar estimates for the length of the backbone segment, or mesh size, but in reality, it is not. It provides crucial information about the mass of polymer that is elastically deformed under swelling, which, as seen in several of our example cases, is a small fraction of the total polymer in the hydrogel. Traditionally, the mass and volume of the branches were lumped with the backbone segment. While this accurately accounted for the polymer mass, it totally neglected the effect of the branches on the interstitial structure of the network and the mobility of solvent and drug molecules inside its voids. This disparity between the length of the chains and their molecular mass in the F−R approach essentially amounts to the visualization of the chains as "fat" linear segments between crosslinks rather than recognize their structurally branched nature.

The effect of branched networks is further highlighted when we analyze the results for the volume ratio f_{BR}. This quantity accounts for the fraction of the interstitial void volume in the network that is taken up by branches. As seen in Table 4, this volume ratio increases, reaching about 9% of the available volume, as the fraction of crosslinker used in the formulation increases. This effect is expected to be even more significant when higher-molecular-weight crosslinkers, and/or higher amounts of crosslinker, are used. This quantity is closely connected with the processes governing diffusion of small molecules through the hydrogel. Its effect should be studied in more depth and correlated with diffusivity coefficients.

3.3. Illustration of the Novel Features of the Approach through Case Comparison. Finally, to better illustrate the power of this novel approach, we present a comparison between two cases involving macromeric crosslinkers of differing molecular weights. To gain even deeper insight, we selected two hydrogels that lead to similar physical expansion phenomena under swelling. Table 5 shows a

https://dx.doi.org/10.1021/acs.biomac.0c01256
Biomacromolecules 2020, 21, 5104−5118

Table 5. Case Study Comparison between Two Systems with Similar Q_v But Different Crosslinker Molecular Weight and Crosslinker Amount

MW_{XC} (g/mol)	f_x	Q_v	M_c (g/mol)	ξ (Å)	ξ_{BB}^{corr} (Å)	ξ_{XC}^{corr} (Å)	ξ_{IC}^{corr} (Å)	ξ_{NC}^{corr} (Å)
575	0.93	10.36	8168.4	40.64	37.59	42.83	68.29	132.78
2000	0.39	10.07	8311.4	24.69	17.87	178.67	35.57	362.56

comparison of two networks with similar Q_v values, one using 93% PEGDA 575 in the precursor formulation and the other using 39% PEGDA 2000. Those two cases happen to be at extreme expansion conditions. Both XC and BB are extended to their maximum lengths.

We first note that the M_c values predicted by F−R for the two samples are similar, in agreement with their similar swelling behavior. Yet, further analysis using the Peppas et al.[35,46−50] approach reveals vastly different mesh sizes for those two sample cases in spite of the similarity of their expansion coefficients. This is a result of the difference in the molecular weight of the repeat unit, M_r, as it is affected by polymer composition and the crosslinker molecular weight.

Clearly, the top-level application of F−R is unable to distinguish the differences in molecular architecture between these two samples. Sole reliance on M_c values will not provide any additional insight into structural differences, naturally because F−R ignores effects related to the crosslinker size. On the other hand, using recommended heuristics based on the calculated mesh size will lead one to limit the PEGDA 2000 sample, which has the smaller mesh dimension, for use in delivery of smaller drug molecules than those usable with the PEGDA 575 sample. This result should be surprising as the two samples not only swell to similar extents but also the one with smaller mesh size is made from larger crosslinker molecules. These observations highlight an enigmatic discrepancy that has been hitherto ignored in the literature.

The approach we propose could help resolve this discrepancy. While the calculated mesh size somewhat approximates the dimension of the BB segment, as seen in Table 5, it does so while completely ignoring the size of the XC segment, thus leading to improper characterization of the network infrastructure. For example, in the PEGDA 2000 case, notice that the XC segment is ∼10 times longer, at full extension, than the BB segment and about 7 times longer than the traditionally calculated mesh size value.

The values of ξ_{IC} and ξ_{NC} presented in Table 5 for the two samples are obviously different and clearly reflect different internal structures and differently shaped spaces. The difference between the two is best understood when visualized using the "idealized" network projection on the $x-z$ plane, introduced in Figure 5b. This projection is presented in Figure 6, where the "channel-like structures" proposed by Figure 5 are recreated for each of the two cases and for two scenarios, one accounting for the crosslinker size and one neglecting it.

Three features of the projections in Figure 6 are worthy of note. First, use of the mesh size as the sole metric to characterize the network might lead to "safe" bounds on the size of encapsulated drugs but will most definitely miss, and misrepresent, the much more complex nature of the network infrastructure. Second, while the swelling behavior of a hydrogel is a good indicator of the degree of crosslinking of the network, as those are inversely related, it is not a sufficient indicator of the shape and structure of its interstitial void space. For example, the two samples presented in Figure 6 swell to similar degrees and have similar "void" volumes but are made of "channels" of widely varying cross-sectional projections. While the approximately rectangular projection of the PEGDA 575 sample has a 2 × 1 aspect ratio, the PEGDA 2000 has an ∼10 × 1 aspect ratio. Third, and based on the last observation, full utilization of the potential of hydrogels made from macromeric crosslinkers requires the realization of the unique features of the forefront drug delivery applications currently under consideration.

Drug molecules were traditionally approximated as either spherical, or coiled spheres, and were usually heavily loaded in the delivery system (particles or slabs) to ensure therapeutic dosage and long-term release. For example, if a drug molecule is selected according to current heuristics for the PEGDA 2000 sample, its diameter would have to be limited to 1/3 the mesh size and so would measure ∼8−10 Å. Based on the visual image reflecting the traditional approach (Figure 6d), this type of drug would fit into that space in moderately small numbers but would move relatively easily through the network. However, when considering the more representative image of the network in Figure 6b, one could see that the actual network has a much higher capacity to encapsulate that small drug up to significantly high concentrations. One could also surmise that the rates of release of that drug from this network would be extremely fast, a problem often encountered and seldom explained. Of course, the presence of branches in that space will relatively affect the generalizations being made here. As shown in Table 3, for the PEGDA 575 case, 87% of the polymer is in branches and the branches occupy 8.5% of the void; for the PEGDA 2000, those values are 91, and 9.1%, respectively. However, despite the presence of branches, the overall trends would still be valid. This all speaks to the grossly underutilized potential of these hydrogels.

If, on the other hand, we consider the large biotherapeutic molecules of interest, such as peptides, proteins, polynucleotides, RNA fragments, plasmids, we must visualize their expected behavior inside a hydrogel. These molecules are often found in conformations that are far from coiled spheres, especially since they are usually highly hydrophilic and exist in the aqueous medium of a hydrogel. We also must consider that the movement of these molecules through the network would involve a series of rearrangements and "negotiations" as they transfer from one "cell" to the next and eventually release into the bulk. These types of molecules will also often require lower therapeutic doses because of the biospecificity of their actions. Every single molecule is capable of initiating a process in the tissue, where it is locally delivered, and create a therapeutic effect. Thus, it is about time that we shift the paradigms of drug encapsulation and delivery and start designing hydrogels using more creative approaches that push the boundaries of mesh dimensions. This will become absolutely necessary when we aim to encapsulate larger and larger molecules; several peptides of interest have molecular weights of a few kilodaltons, but some of the other biomolecules, including small RNA fragments, could easily reach 100 kDa. If a molecule is chain-like, or has an elongated aspect ratio, it

https://dx.doi.org/10.1021/acs.biomac.0c01256
Biomacromolecules 2020, 21, 5104−5118

would not make sense to attempt to have a space large enough for it to fully gyrate. When spaces inside hydrogels are designed according to such criteria, the mechanical properties of the hydrogel will be severely compromised. Thus, we believe that the greatest contribution of macromeric crosslinkers is in creating the types of spaces that could contain these biomolecules of nontraditional shapes and sizes. Of course, the challenge would be to balance this against the need for reasonable rates, and times, of release. The analysis we provide here could be used to hypothesize about the relation of molecular architecture design in hydrogel networks to the size and shape of encapsulated drugs, but this issue will not be fully understood until properly designed experiments are conducted and validated. Just as heuristics have been used traditionally, we could use the predicted values of ξ_{IC} and ξ_{NC} to establish initial bounds on the molecules and then iteratively measure rates of release until a proper balance is reached.

4. CONCLUSIONS

In this paper, a new approach to characterizing the molecular architecture, and determine the mesh dimensions, of cross-linked polymer networks was developed. By making use of the Flory−Rehner approach as the starting point, the theory was expanded to make it applicable to networks with macromeric crosslinking monomers and to networks with high concentrations of the crosslinker.

By identifying that the thermodynamic analysis of the Flory−Rehner theory is fundamentally calculating the total number of effectively elastic segments, we were able to define a surrogate segment, λ, encompassing one backbone segment and half of a crosslinker segment to associate with those elastically effective segments. This new construct allows the calculation of a corrected total molecular weight in between crosslinks—excluding the crosslinker and subsequently to the proper distribution of that molecular mass between backbone segments and branches. This then leads to the ability to calculate the length of all types of segments in the hydrogel.

A 3D model for the visualization of the network based on this approach led to the observation of network "channel-like structures". These "channels" can be properly quantified through two new dimension variables, termed the intrachain mesh dimension and the interchain mesh dimension. These dimensions establish bounds on the maximum size of molecules that can be encapsulated in a specific network and provide insight into the suitability of the hydrogel for molecules with specific shapes and/or aspect ratios. Furthermore, the explicit accounting of branch segments (BR) provides additional insight into the skeletal structure of the network and the impact of the branches on the interstitial space and the mobility of drug molecules within it. The newly introduced variable, f_{BR}, accounts for the fraction of the void volume in the polymer network taken up by branches. We hypothesize that molecules with dimensions as large as ξ_{IC} and ξ_{NC} are potentially able to fit inside the network, but as the value of f_{BR} increases, their diffusion in or out of the network will be significantly hampered.

In future publications, we plan to explore how to utilize the equations presented here to back-calculate the hydrogel formulations needed for successful encapsulation and release of specific therapeutics of different sizes. By adjusting the hydrogel mesh properties, one can also expect to be able to alter and control the release kinetics of such therapeutics.

We will explore alternatives to increase mesh dimensions without using extremely high-molecular-weight crosslinkers, as is commonly done, to minimize levels of branching if needed. When branching is significant, we also aim to better quantify the effect of BR segments on diffusion of drug molecules. Ideally, one would be able to correlate the mesh dimensions, the size of the molecule to be encapsulated, and the volume taken up by branches to a certain diffusion profile and diffusivity. However, more experimentation is still needed to elaborate such correlations.

It should be stressed that the approach of this article was developed with emphasis on macromeric crosslinkers that are bifunctional in nature. Several other arrangements, also involving complex molecular architecture, have been explored in the past decade through the use of multifunctional crosslinkers, e.g., multiarm PEG with either four- or eight-arm configuration, and utilizing step-growth mechanisms for crosslinking, such as click chemistry and Michael addition-type reactions.[45,64−67] Our approach could be adapted for the characterization of the complex molecular architecture of these novel hydrogels and could greatly enhance their understanding. However, we must point out that a critical re-derivation of the steps involved in the approach needs to be carried out to develop the proper equations for each case individually. The starting point of such derivation will rely on the correct identification of the basic representative cell and the classification of its segments as elastically deformable or not, and the establishment of relational operators that represent the geometric dependencies among these segments.

AUTHOR INFORMATION

Corresponding Author

Fouad Teymour − *Department of Chemical and Biological Engineering, Illinois Institute of Technology, Chicago, Illinois 60616, United States;* orcid.org/0000-0002-8366-7956; Email: teymour@iit.edu

Authors

Fernando T. P. Borges − *Department of Chemical and Biological Engineering, Illinois Institute of Technology, Chicago, Illinois 60616, United States*

Georgia Papavasiliou − *Department of Biomedical Engineering, Illinois Institute of Technology, Chicago, Illinois 60616, United States*

Complete contact information is available at: https://pubs.acs.org/10.1021/acs.biomac.0c01256

Notes

The authors declare no competing financial interest.

ACKNOWLEDGMENTS

This work was financially supported by the National Institutes of Health Grant number R21AI124037-01 (awarded to G.P., PI).

REFERENCES

(1) Caló, E.; Khutoryanskiy, V. V. Biomedical applications of hydrogels: A review of patents and commercial products. *Eur. Polym. J.* **2015**, *65*, 252−267.

(2) Peppas, N. A.; Bures, P.; Leobandung, W.; Ichikawa, H. Hydrogels in pharmaceutical formulations. *Eur. J. Pharm. Biopharm.* **2000**, *50*, 27−46.

(3) Orive, G.; Hernandez, R. M.; Gascon, A. R.; Domınguez-Gil, A.; Pedraz, J. L. Drug delivery in biotechnology: present and future. *Curr. Opin. Biotechnol.* **2003**, *14*, 659−664.
(4) Wichterle, O.; Lim, D. Hydrophilic gels for biological use. *Nature* **1960**, *185*, 117.
(5) Chen, X.; Martin, B. D.; Neubauer, T. K.; Linhardt, R. J.; Dordick, J. S.; Rethwisch, D. G. Enzymatic and chemoenzymatic approaches to synthesis of sugar-based polymer and hydrogels. *Carbohydr. Polym.* **1995**, *28*, 15−21.
(6) Kashyap, N.; Kumar, N.; Kumar, M. Hydrogels for pharmaceutical and biomedical applications. *Crit. Rev. Ther. Drug Carrier Syst.* **2005**, *22*, 107−149.
(7) Hiratani, H.; Alvarez-Lorenzo, C. The nature of backbone monomers determines the performance of imprinted soft contact lenses as timolol drug delivery systems. *Biomaterials* **2004**, *25*, 1105−1113.
(8) Williams, C. An investigation of the benefits of Aquacel Hydrofibre wound dressing. *Br. J. Nurs.* **1997**, *6*, 494−496.
(9) Thomas, S.; Jones, H. Clinical experiences with a new hydrogel dressing. *J. Wound Care* **1996**, *5*, 132−133.
(10) Corkhill, P. H.; Hamilton, C. J.; Tighe, B. J. Synthetic hydrogels VI. Hydrogel composites as wound dressings and implant materials. *Biomaterials* **1989**, *10*, 3−10.
(11) Bryant, S. J.; Anseth, K. S. The effects of scaffold thickness on tissue engineered cartilage in photocrosslinked poly (ethylene oxide) hydrogels. *Biomaterials* **2001**, *22*, 619−626.
(12) Mann, B. K.; Gobin, A. S.; Tsai, A. T.; Schmedlen, R. H.; West, J. L. Smooth muscle cell growth in photopolymerized hydrogels with cell adhesive and proteolytically degradable domains: synthetic ECM analogs for tissue engineering. *Biomaterials* **2001**, *22*, 3045−3051.
(13) Liu, V. A.; Bhatia, S. N. Three-dimensional photopatterning of hydrogels containing living cells. *Biomed. Microdevices* **2002**, *4*, 257−266.
(14) Nguyen, K. T.; West, J. L. Photopolymerizable hydrogels for tissue engineering applications. *Biomaterials* **2002**, *23*, 4307−4314.
(15) Schmedlen, R. H.; Masters, K. S.; West, J. L. Photocrosslinkable polyvinyl alcohol hydrogels that can be modified with cell adhesion peptides for use in tissue engineering. *Biomaterials* **2002**, *23*, 4325−4332.
(16) Smeds, K. A.; Grinstaff, M. W. Photocrosslinkable polysaccharides for in situ hydrogel formation. *J. Biomed. Mater. Res.* **2001**, *54*, 115−121.
(17) Mason, M. N.; Metters, A. T.; Bowman, C. N.; Anseth, K. S. Predicting controlled-release behavior of degradable PLA-b-PEG-b-PLA Hydrogels. *Macromolecules* **2001**, *34*, 4630−4635.
(18) Lu, S.; Anseth, K. S. Photopolymerization of multilaminated poly (HEMA) hydrogels for controlled release. *J. Controlled Release* **1999**, *57*, 291−300.
(19) Lu, S.; Ramirez, W. F.; Anseth, K. S. Photopolymerized, multilaminated matrix devices with optimized nonuniform initial concentration profiles to control drug release. *J. Pharm. Sci.* **2000**, *89*, 45−51.
(20) Uhrich, K. E.; Cannizzaro, S. M.; Langer, R. S.; Shakesheff, K. M. Polymeric systems for controlled drug release. *Chem. Rev.* **1999**, *99*, 3181−3198.
(21) Vadlamudi, S.; Nichols, D.; Papavasiliou, G.; Teymour, F. Phosphate-loaded hydrogel nanoparticles for sepsis prevention prepared via inverse miniemulsion polymerization. *Macromol. React. Eng.* **2019**, *13*, No. 1800066.
(22) Yin, Y.; Papavasiliou, G.; Zaborina, O. Y.; Alverdy, J. C.; Teymour, F. De novo synthesis and functional analysis of polyphosphate-loaded poly(ethylene) glycol hydrogel nanoparticles targeting pyocyanin and pyoverdin production in pseudomonas aeruginosa as a model intestinal pathogen. *Ann. Biomed. Eng.* **2017**, *45*, 1058.
(23) Nichols, D.; Pimentel, M. B.; Borges, F. T. P.; Hyoju, S. K.; Teymour, F.; Hong, S. H.; Zaborina, O.; Alverdy, J. C.; Papavasiliou, G. Sustained release of phosphates from hydrogel nanoparticles suppresses bacterial collagenase and biofilm formation in vitro. *Front. Biotechnol.* **2018**, *7*, No. 153.
(24) Borges, F. T. P.; Papavasiliou, G.; Teymour, F. Synthesis of polyphosphate-loaded nanoparticles using inverse miniemulsion polymerization for sustained delivery to the gastrointestinal tract. *Macromol. React. Eng.* **2019**, *13*, No. 1800068.
(25) Pimentel, M. B.; Borges, F. T. P.; Fang, K.; He, Y.; Staneviciute, A.; Teymour, F.; Hong, S. H.; Zaborina, O. Y.; Alverdy, J. C.; Papavasiliou, G. An in vitro tissue model for screening sustained release of phosphate-based therapeutics in attenuating pathogen-induced proteolytic matrix degradation. *J. Mater. Chem. B* **2020**, *8*, 2454.
(26) Young, D. A.; Pimentel, M. B.; Lima, L. D.; Custodio, A. F.; Lo, W. C.; Chen, S. C.; Teymour, F.; Papavasiliou, G. Design and characterization of hydrogel nanoparticles with tunable network characteristics for sustained release of a VEGF-mimetic peptide. *Biomater. Sci.* **2017**, *5*, 2079−2092.
(27) Mansour, S. C.; de la Fuentes-Nunez, C.; Hancock, R. E. W. Peptide IDR-1018: modulating the immune system and targeting bacterial biofilms to treat antibiotic-resistant bacterial infections. *J. Pept. Sci.* **2015**, *21*, 323−329.
(28) Wang, Y.; Malcolm, D. W.; Benoit, D. S. W. Controlled and sustained delivery of siRNA/NPs from hydrogels expedites bone fracture healing. *Biomaterials* **2017**, *139*, 127−138.
(29) McGill, J. L.; Kelly, S. M.; Kumar, P.; Speckhart, S.; Haughney, S. L.; Henningson, J.; Narasimhan, B.; Sacco, R. E. Efficacy of mucosal polyanhydride nanovaccine against respiratory syncytial virus infection in the neonatal calf. *Sci. Rep.* **2018**, *8*, No. 3021.
(30) Thukral, A.; Ross, K.; Hansen, C.; Phanse, Y.; Narasimhan, B.; Steinberg, H.; Talaat, A. M. A single dose polyanhydride-based nanovaccine against paratuberculosis infection. *npj Vaccines* **2020**, *5*, No. 15.
(31) Schrijver, R. S.; Langedijk, J. P. M.; Keilf, G. M.; Middel, W. G. J.; Maris-Veldhuis, M.; Van Oirschot, J. T.; Rijsewijk, F. A. M. Comparison of DNA application methods to reduce BRSV shedding in cattle. *Vaccine* **1998**, *16*, 130−134.
(32) Flory, P. J.; Rehner, J. Statistical mechanics of crosslinked polymer networks I. Rubberlike elasticity. *J. Chem. Phys.* **1943**, *11*, 512−520.
(33) Flory, P. J.; Rehner, J. Statistical mechanics of crosslinked polymer networks II. Swelling. *J. Chem. Phys.* **1943**, *11*, 521−526.
(34) Flory, P. J. Statistical mechanics of swelling of network structures. *J. Chem. Phys.* **1950**, *18*, 108−111.
(35) Canal, T.; Peppas, N. A. Correlation between mesh size and equilibrium degree of swelling of polymeric network. *J. Biomed. Mater. Res.* **1989**, *23*, 1183−1193.
(36) Elbert, D. L.; Hubbell, J. A. Conjugate addition reactions combined with free-radical cross-linking for the design of materials for tissue engineering. *Biomacromolecules* **2001**, *2*, 430−441.
(37) Borges, F. T. P.; Papavasiliou, G.; Murad, S.; Teymour, F. Effect of phosphate salt concentration and solution pH on the aqueous-phase homo and copolymerization of n-vinyl pyrrolidone. *Macromol. React. Eng.* **2018**, *12*, No. 1800012.
(38) Lee, C. Y.; Teymour, F.; Camastral, H.; Tirelli, N.; Hubbell, J. A.; Elbert, D. L.; Papavasiliou, G. Characterization of the network structure of PEG diacrylate hydrogels formed in the presence of n-vinyl pyrrolidone. *Macromol. React. Eng.* **2014**, *8*, 314−328.
(39) Watkins, A. W.; Anseth, K. S. Investigation of molecular transport and distributions in poly(ethylene glycol) hydrogels with confocal laser scanning microscopy. *Macromolecules* **2005**, *38*, 1326−1334.
(40) Kalakkunnath, S.; Kalika, D. S.; Lin, H.; Freeman, B. D. Viscoelastic characteristics of UV polymerized poly(ethylene glycol) diacrylate networks with varying extents of crosslinking. *J. Polym. Sci., Part B: Polym. Phys.* **2006**, *44*, 2058−2070.
(41) Valentín, J. L.; Carretero-Gonzalez, J.; Mora-Barrantes, I.; Chasse, W.; Saalwachter, K. Uncertainties in the determination of cross-link density by equilibrium swelling experiments in natural rubber. *Macromolecules* **2008**, *41*, 4717−4729.

https://dx.doi.org/10.1021/acs.biomac.0c01256
Biomacromolecules 2020, 21, 5104−5118

(42) Nandi, S.; Winter, H. H. Swelling behavior of partially cross-linked polymers: A ternary system. *Macromolecules* **2005**, *38*, 4447−4455.
(43) Edgecombe, S.; Schneider, S.; Linse, P. Monte Carlo simulations of defect-free cross-linked gels in the presence of salt. *Macromolecules* **2004**, *37*, 10089−10100.
(44) Padmavathi, N. C.; Chatterji, P. R. Structural characteristics and swelling behavior of poly(ethylene glycol) diacrylate hydrogels. *Macromolecules* **1996**, *29*, 1976−1979.
(45) Truong, V.; Blakey, I.; Whittaker, A. K. Hydrophilic and amphiphilic polyethylene glycol-based hydrogels with tunable degradability prepared by "click" chemistry. *Biomacromolecules* **2012**, *13*, 4012−4021.
(46) Peppas, N. A.; Barr-Howell, B. D. Characterization of the Cross-Linked Structure of Hydrogels. *Hydrogels in Medicine and Pharmacy: Fundamentals*; Taylor and Francis Group, LLC, 1986; Chapter 2, pp 27−56.
(47) Korsmeyer, R. W.; Peppas, N. A. Effect of the morphology of hydrophilic polymeric matrices on the diffusion and release of water soluble drugs. *J. Membr. Soc.* **1981**, 211−227.
(48) Bell, C. L.; Peppas, N. A. Water, solute and protein diffusion in physiologically responsive hydrogels of poly(methacrylic-acid-g-ethylene glycol). *Biomaterials* **1996**, *17*, 1203−1218.
(49) Peppas, N. A.; Hilt, J. Z.; Khademhosseini, A.; Langer, R. Hydrogels in Biology and Medicine: From Molecular Principles to Bionanotechnology. *Adv. Mater.* **2006**, *18*, 1345−1360.
(50) Slaughter, B. V.; Khurshid, S. S.; Fisher, O. Z.; Khademhosseini, A.; Peppas, N. A. Hydrogels in Regenerative Medicine. *Adv. Mater.* **2009**, *21*, 3307−3329.
(51) Weber, L. M.; He, J.; Bradley, B.; Haskins, K.; Anseth, K. S. PEG-based hydrogels as an in vitro encapsulation platform for testing controlled b-cell microenvironments. *Acta Biomater.* **2006**, *2*, 1−8.
(52) Benoit, D. S. W.; Nuttelman, C. R.; Collins, S. D.; Anseth, K. S. Synthesis and characterization of a fluvastatin-releasing hydrogel delivery system to modulate hMSC differentiation and function for bone regeneration. *Biomaterials* **2006**, *27*, 6102−6110.
(53) Rehmann, M. S.; Skeens, K. M.; Kharkar, P. M.; Ford, E. M.; Maverakis, E.; Lee, K. H.; Kloxin, A. M. Tuning and Predicting Mesh Size and Protein Release from Step Growth Hydrogels. *Biomacromolecules* **2017**, *18*, 3131−3142.
(54) Li, W. H.; Hamielec, A. E.; Crowe, C. M. Kinetics of the free-radical copolymerization of methyl methacrylate/ethylene glycol dimethacrylate: 1. Experimental investigation. *Polymer* **1989**, *30*, 1513−1517.
(55) Kizilel, S.; Papavasiliou, G.; Gossage, J.; Teymour, F. Mathematical model for vinyl-divinyl polymerization. *Macromol. React. Eng.* **2007**, *1*, 587−603.
(56) Millar, J. R.; Smith, D. G.; Marr, W. E.; Kressman, T. R. E. Solvent-modified polymer networks. Part I. The preparation and characterisation of expanded-network and macroporous styrene−divinylbenzene copolymers and their sulphonates. *J. Chem. Soc.* **1963**, 218−225.
(57) Sederel, W. L.; De Jong, G. J. Styrene−divinylbenzene copolymers. Construction of porosity in styrene divinylbenzene matrices. *J. Appl. Polym. Sci.* **1973**, *17*, 2835−2846.
(58) Borges, F. T. P. Development of Fully Biocompatible Hydrogel Nanoparticle Formulations for Controlled-Release Delivery of a Wide Variety of Biomolecules. Doctoral Dissertation, Illinois Institute of Technology: Chicago, 2020.
(59) Brandrup, J.; Immergut, E. H. Solution Properties. *Polymer Handbook*; Wiley Interscience: New York, 1989, Chapter VII.
(60) Rubinstein, M.; Colby, R. H. *Polymer Physics*; Oxford University Press: New York, 2003.
(61) Teymour, F.; Campbell, J. D. Analysis of the dynamics of gelation in polymerization reactors using the "numerical fractionation" technique. *Macromolecules* **1994**, *27*, 2460−2469.
(62) Merrill, E. W.; Dennison, K. A.; Sung, C. Partitioning and diffusion of solutes in hydrogels of poly(ethylene oxide). *Biomaterials* **1993**, *14*, 1117−1126.
(63) Millipore Sigma. Product Data Sheet, Oct 21, 2020. https://www.sigmaaldrich.com/catalog/product/aldrich/437441.
(64) Jivan, F.; Fabela, N.; Davis, Z.; Alge, D. L. Orthogonal click reactions enable the synthesis of ECM-mimetic PEG hydrogels without multi-arm precursors. *J. Mater. Chem. B* **2018**, *6*, 4929−4936.
(65) Shih, H.; Lin, C. C. Cross-Linking and Degradation of Step-Growth Hydrogels Formed by Thiol−Ene Photoclick Chemistry. *Biomacromolecules* **2012**, *13*, 2003−2012.
(66) Tan, H.; DeFail, A. J.; Rubin, J. P.; Chu, C. R.; Marra, K. G. Novel multiarm PEG-based hydrogels for tissue engineering. *J. Biomed. Mater. Res., Part A* **2010**, *92A*, 979−987.
(67) Kim, J.; Kong, Y. P.; Niedzielski, S. M.; Singh, R. K.; Putnam, A. J.; Shikanov, A. Characterization of the crosslinking kinetics of multi-arm poly(ethylene glycol) hydrogels formed via Michael-type addition. *Soft Matter* **2016**, *12*, 2076−2085.

https://dx.doi.org/10.1021/acs.biomac.0c01256
Biomacromolecules 2020, 21, 5104−5118